Composites & nanocomposites

Advances for enhancing the electrical properties and microhardness activity of ZnO/Cu/ZnO thin films prepared by ALD

S. S. Fouad[1], L. I. Soliman[2], E. Baradács[3,4], M. E. Sayed[5], B. Parditka[4], N. F. Osman[5], M. Nabil[6,*] , and Zoltán Erdélyi[4]

[1] Department of Physics, Faculty of Education, Ain Shams University, Cairo 11566, Egypt

[2] Depaetment of Solid-State Physics, National Research Centre, Physics Research Institute, Cairo, Egypt

[3] Departement of Environmental Physics, Faculty of Science and Technology, University of Debrecen, Poroszlay U.6, Debrecen 4026, Hungary

[4] Departement of Solid- State Physics, Faculty of Science and Technology, University of Debrecen, P.O. Box 400, Debrecen 4002, Hungary

[5] Basic Science Department, Modern Academy for Engineering and Technology in Maadi, Cairo, Egypt

[6] Department of Basic Engineering Sciences, Faculty of Engineering (Shoubra), Benha University, Benha, Egypt

ABSTRACT

Substantial consideration is being devoted to the innovation of AC Conductivity, sheet resistance measurements and Microhardness as a function of Cu interlayer thickness of conductive ZnO/Cu/ZnO thin films. ZnO layer was successfully prepared via atomic layer deposition (ALD), while Cu interlayer was deposited by Dc magnetron sputtering. The combination of ZnO/Cu/ZnO with constant ZnO thickness (70 nm) and variable Cu interlayer thickness (20, 50 and 70 nm), has its own individuality in enhancing the performance of the electrical and mechanical properties. The proposed methodology based on the previously published data of the structural characterization, proved to be very effective. The study of (XRD) and (SEM) revealed an increase in particle size with the increase in Cu content. The outcome of the absorption measurements supports the existence of allowed direct transition for ZnO/Cu/ZnO thin films, and the optical energy gap is strongly dependent on the amount of Cu interlayer thickness. The AC conductivity is explored in the frequency range of (1 MHz–1 GHz) and the temperature range of (293 to 423 K). At different frequencies AC conductivity measurements demonstrate a decrement with the increment of Cu content. An agreement between experimental and theoretical results suggests that the behavior of AC conductivity can be successfully explained by Correlated Barrier Hopping (CBH) model, to elucidate the conduction mechanism

existing in our ZnO/Cu/ZnO system. A superior combination between mechanical and electrical properties was evaluated by Vickers hardness and the 4-point technique. The obtained results demonstrate that the layer thickness and the layer thickness ratio of ZnO and Cu are the important parameters which are responsible for the improvement of structural, electrical and mechanical properties of ZnO/Cu/ZnO multilayer films. These findings pave the way for the future development of novel energy devices and photocatalytic and absorption applications.

Introduction

Recently, extensive attention has been given to the development of multilayer thin films with high electrical conductivity as well as high transparency and high reflectivity as they possess superior properties when compared with the conventionally used ones [1–3].

Practical applications of transparent conducting coatings increase after the introduction of wide band gap semi-conducting films. ZnO is a good semiconductor material and is particularly attractive because of its wide direct band gap of 3.37 eV, and higher excitonic binding energy (-60 meV) at room temperature [4]. Many oxide materials such as TiO_2, SnO_2, ZnS, Nb_2O_5 have been widely used as dielectric layers. Some metal materials are suitable for the mid-layer structure, such as Au, Ag, Cu, Al etc. Doped ZnO is an attractive electrode material for solar cell applications and one of the bases of various smart and functional materials for transparent conducting oxide (TCO).

ZnO and TiO_2 materials that are supported by metal transition material such as Cu as the mid-layer has been verified as an effective method which mainly arise from doping-induced band gap modification [5–8]. Cu material effectively been a useful material due to its low cost and low resistivity, and it tends to be easily prepared and used as interlayer comparing with Au, Al and Ag metals [2, 9–14]. Practically, ZnO-based thin film can be grown by various techniques such as atomic layer deposition (ALD) [2, 15] thermal evaporation [16, 17], chemical vapor deposition [18], spray pyrolysis [19], sol–gel process [20], pulsed laser deposition [21], electron beam deposition [22] and sputtering [23]. Farther more, excellent physical properties can be obtained by optimizing Cu mid-layer thickness and suitable ZnO layer thickness. These materials are useful due to the simple structure of the ZnO network and the high mobility of cupper, which can be used for energy storage devices and solid-state batteries [24]. Measurements on ionic materials give useful information about dynamical processes involving ionic motion.

Therefore, the aim of this literature study is to show clearly the effect of the thickness of Cu as an interlayer, on the AC conductivity, electrical, and mechanical properties of ZnO/Cu/ZnO multilayer thin films. From theses analyses, several applications could be suggested.

Experimental procedures

We have fabricated the three samples of S1(ZnO/Cu_{20}/ZnO), S2 (ZnO/Cu_{50}/ZnO) and S3(ZnO/Cu_{70}/ZnO) on a glass and SiO_2 substrates. In this type of sandwich structured, the ZnO thin films were used as top and bottom layers and were deposited with constant thickness via atomic layer deposition (ALD), which is one of the most powerful techniques in preparing various multilayer oxides, because of its surface—controlled and chemically stable process offering high uniformity in film growth [25]. The Cu layer inserted between top and bottom oxide layers was deposited via Dc magnetron sputtering at 200 °C. The details of the preparation and morphological studies including the grazing incident X-Ray diffraction (GIXRD) patterns, scanning electron microscope (SEM), crystallite sizes, and the roughness were given in details in [15]. The thickness of S1, S2 and S3 was precisely controlled through the number of the ALD cycles and checked by a profilometer (AMBIOS XP-1) and a spectroscopic ellipsometer (Semilab SE-2000). During the fitting of the X-ray reflectivity (XRR) measurements, the thickness of the

Springer

native of SiO$_2$ layer was kept constant, since we measured it on bare substrate (without the ZnO/Cu/ZnO tri-layer) with a spectroscopic ellipsometer and evaluated it for more accurate evaluation of the XRR measurements. The GIXRD patterns of S1, S2 and S3 grown on Si (100) are shown in Fig. 1.

As seen the GIXRD pattern show good similarity, between the three samples, the only difference that appears is the ration among the intensity of the individual peaks. The higher intensity is seen on the (002) peak for S3, and a large crystallite size corresponding to the full width at half maximum (FWHM) values than that for S1and S2. The observed increase in the intensity of the peak belong to Cu (111) indicates that the preferential growth of the sputtered Cu interlayer is strongly affected by the variation of the thickness of the Cu. The calculated crystallite sizes of the three samples are given in details in Table 1.

For further investigation we also used the data measured by the spectroscopic ellipsometer and profilometer, furthermore performed X-ray reflectivity (XRR) measurements. From these measurements, we were able to determine the accurate thickness and average value of the surface roughness ± 3 nm and the results are summarized for S1, S2 & S3 in details in Table 2.

In the following SEM Images for the three types of samples with 100,000 × and 50,000 × magnification, shown in Fig. 2. In case of S2 & S3 the surface shows a homogeneous ZnO coverage while the surface of S1 show segmented coverage. The underlying Cu Layer

is obscured by the topmost crystalline ZnO layer. Theoretically the shape factor can be in the range of 0.68–2.08, so as seen changing the value of the shape factor did not change the crystallite size significantly. The optical energy gap, optical density, skin depth, metallization criterion and the reflection loss function were also calculated, for S1, S2 and S3 and are given in details in [15].

The above determined results confirmed the improvement of the film quality with increasing the Cu concentration. The AC conductivity of the prepared samples was carried out in the temperature range (303- 473 K) and the frequency range of (1 MHz–1 GHz). The sample temperature was measured and controlled by using a calibrated Chromel–Alumel thermocouple connected to (TCN4M-24R Aulonics—Korea) temperature controller. For AC conductivity measurements, a programmable automatic LCR bridge (Wide range frequencies between 1 MHz and 1 GHz, Keysight—E4991B impedance analyzer (NOVOCONTROL) was used. The sheet resistance was measured at room temperature for the prepared samples by using 4-point Probes Resistivity Measurement System over a period 15 s. The microhardness process is fairly similar to the normal Vickers hardness test. The Vickers microhardness was measured by using Japan's Shimadzu microhardness tester hp m—2E (344—04,109–22) Tester with a force of 1.96 N over a period of 15 s. Normally, the entire load is applied for 10 to 15 s for each sample. The Vickers hardness were calculated by

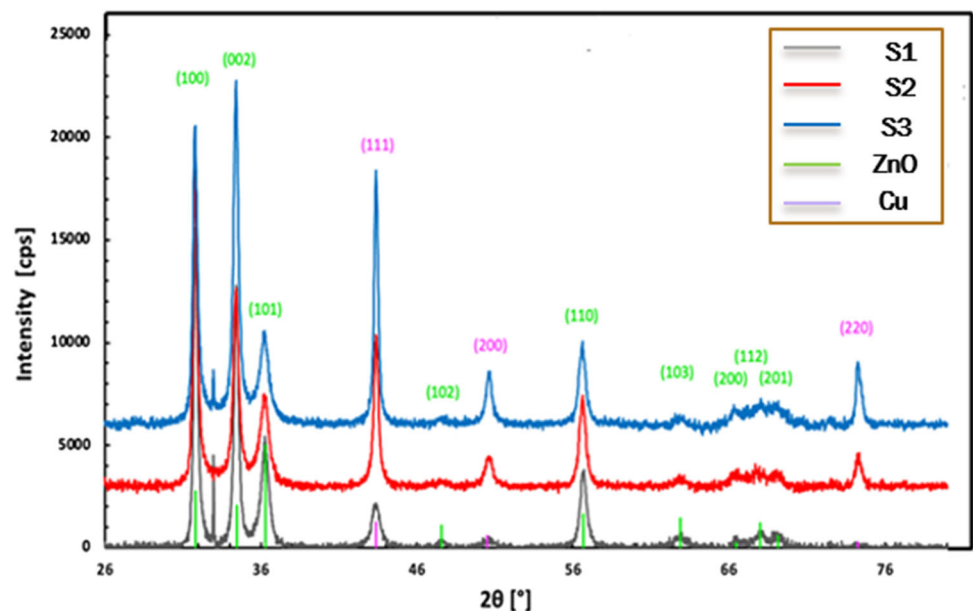**Figure 1** GIXRD diffraction patterns of S1, S2 and S3 thin films.

Table 1 Crystallite size of Cu for the studied S1, S2 and S3 respectively

Samples	$2\theta^0$ (Cu)	Radian (θ^0) (Cu)	Cos Radian (θ^0) (Cu)	β^0 (FWHM)	Radian β^0	D Crystallite size (nm)
S1	43.48	0.3794	0.9289	0.99	0.017278	8.64
S2	43.432	0.3790	0.9290	0.737	0.012863	11.60
S3	43.466	0.3793	0.9289	0.71	0.012391	12.05

Table 2 Thickness and roughness for S1, S2 and S3 respectively

Samples Layer	S1		S2		S3	
	Thickness [nm]	Roughness [nm]	Thickness [nm]	Roughness [nm]	Thickness [nm]	Roughness [nm]
ZnO	74.3 ± 0.4	3.0 ± 0.04	71.8 ± 0.3	2.2 ± 0.09	74.3 ± 0.13	1.8 ± 0.02
Cu	19.8 ± 0.4	3.8 ± 0.12	49.5 ± 0.7	2.4 ± 0.2	70.4 ± 0.3	2.3 ± 0.04
ZnO	76.0 ± 1.3	3.6 ± 0.1	74.3 ± 1	2.0 ± 0.08	76.2 ± 3	3.0 ± 0.13
SiO_2	2.40	0.8 ± 0.004	2.40	0.5 ± 0.07	2.40	0.0 ± 0.2

Figure 2 SEM image for **a**, **a1**, **b**, **b1** and **c**, **c1** for S1, S2 and S3 with high and low magnification.
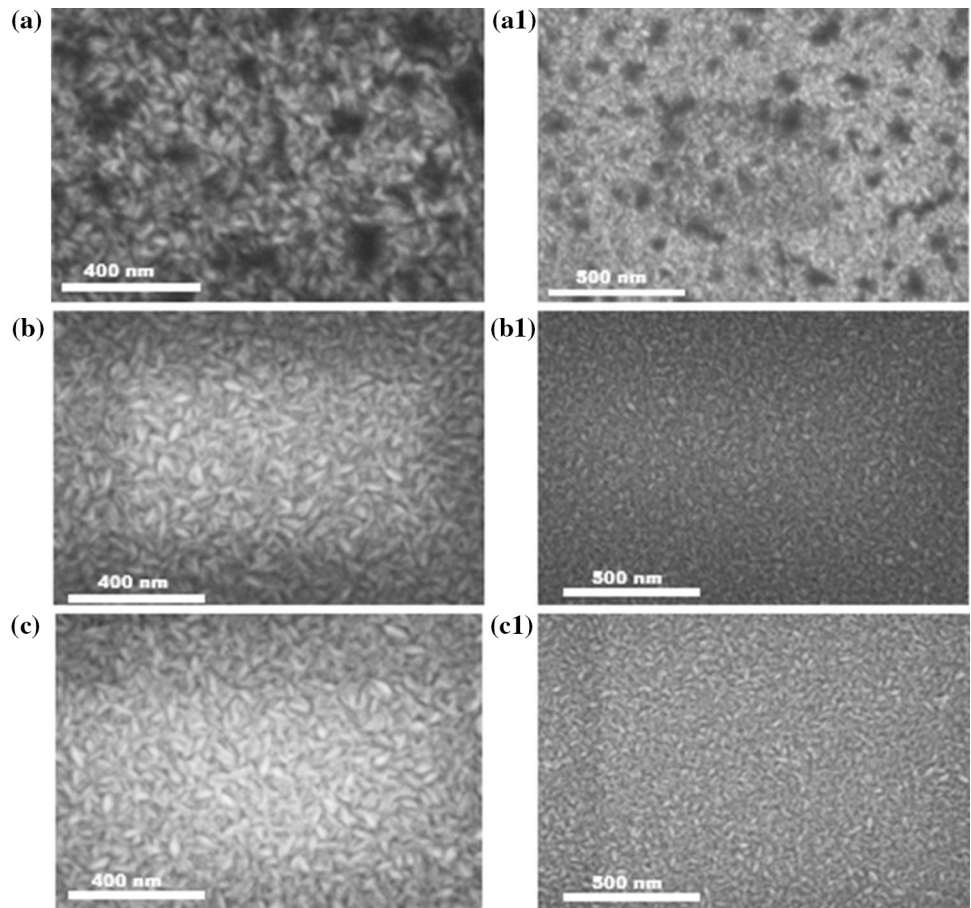
dividing the load by the indentation's square millimeter area. The Vickers test can be used for all metals and coating films [26] and has one of the widest scales among hardness tests. The unit of hardness given by the test is known as the Vickers Pyramid Number (HV) or Diamond Pyramid Hardness (DPH) Phase diagram is a graphical presentation of the physical state of any substance under different condition of temperature and pressure, it is also providing the relationship between phases in any composition. The phase diagram of S1, S2 and S3 is given in Fig. 3.

Results and discussion

AC conductivity and mechanism

AC conductivity provides several information on different relaxation mechanisms by studying the evolution of conductivity as a function of frequency and temperature. In general, measuring the conductivity accurately is necessary for quality control and process monitoring. Due to localized states, the AC conductivity (σ_{ac}) in polycrystalline materials can be described by [3–13]:

$$\sigma_{ac}(\omega) = \sigma_t - \sigma_{dc} \tag{1}$$

where σ_t, σ_{dc} total conductivity and DC conductivity respectively. Since the σ_{dc} is small as compared to σ_{ac} in our ZnO/Cu/ZnO thin film system, the σ_t can be considered to be equal σ_{ac}. Generally, it has been reported that, the AC conductivity depends on frequency and can derived by the following equation [11]:
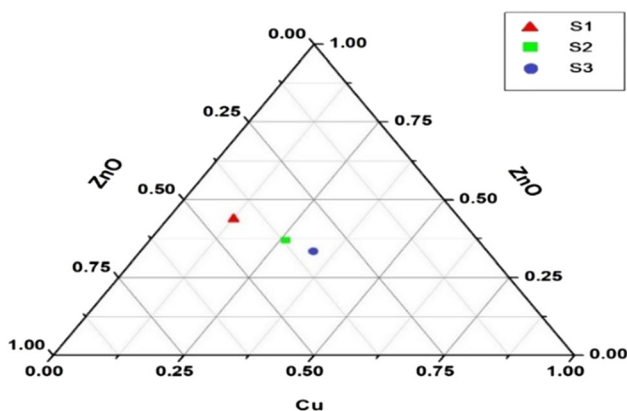

Figure 3 Phase diagram for S1, S2 and S3 thin films.

$$\sigma_{ac} = A\omega^s \tag{2}$$

where A is a constant, ω is the angular frequency and (s) is the frequency exponent which is generally less than 1 or equal one and is frequency and temperature dependent. The obtained results of the dependence of σ_{ac} as a function of frequency in the range (1 MHz—1 GHz) over a constant working temperature (293–423 K) is shown in Fig. 4a, b, c for S1, S2 and S3. It appears that the there is a rise in AC conductivity with increasing frequency, and at higher temperature the conductivity becomes independent of temperature in the high frequencies range. Such performance of σ_{as} suggests that the relocation of ions occurs in the substances due to their migration at low frequencies [8]. The behavior can be expressed by the relation given in Eq. (2).

The increase in the applied frequency enhances the hopping of charge carriers between the localized states [5]. From the slope of the linear part at higher frequencies at different temperature given in Fig. 5 for S1, S2 and S3, we determine the different values of the exponent (s). The temperature dependence of the frequency exponent for S1, S2 and S3 are presented in Fig. 5a. As observed $0.975 \leq s \leq 0.995$, is less than unity and decreases with the increase in temperature. Such behavior proves that the conduction mechanism can be modeled by the correlated barrier hopping mode (CBH).

The exponent (s) was also derived on the basis of the model given by Elliott [27].

$$s = 1 - (6K_B T/E_g) \tag{3}$$

where E_g is the bandgap energy for S1, S2 and S3 given previously in [15] and are presented in Table 3. The obtained results of (s) given in Fig. 5a and b, gave a second prove that the behavior of ZnO/Cu/ZnO system can be successfully explained by correlated barrier hopping (CBH) model as shown in many other studies [11–13]. According to (CBH), (s) can be written as [28]:

$$1 - s = 6KT/[W_m + KT \ln(\omega\tau_o)] \tag{4}$$

where τ_o *is the relaxation time*, $(\tau_o = 10^{-12})$. In such approximation, the exponent (s) tend to be unity for large values of ($Wm = KT$) and Eq. (4) can be simplified as [28].
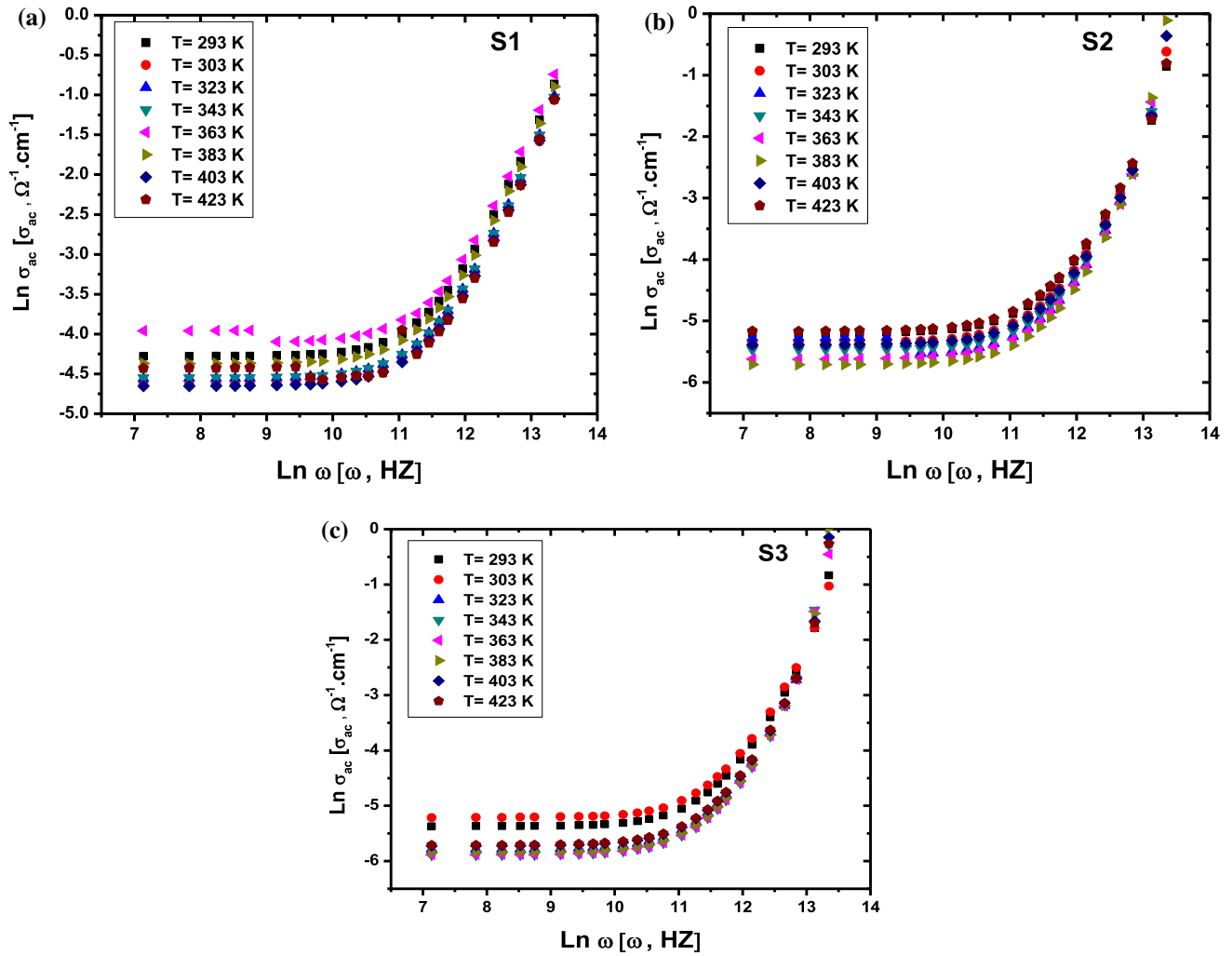
$$1 - s = 6KT/Wm \tag{5}$$

Figure 4 Ln σ_{ac} versus ln ω at different temperatures of **a** S1, **b** S2 and **c** S3 samples.
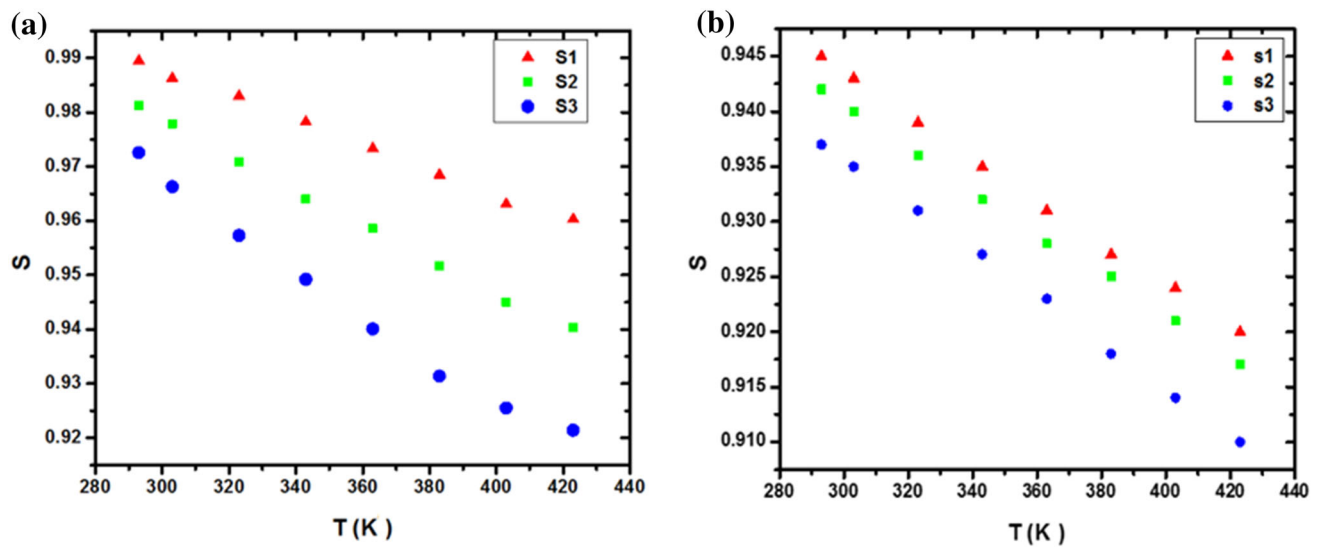

Figure 5 Frequency exponent (s) **a** from Eq. (2), **b** from Eq. (3)..

Table 3 Values of optical energy gap (E_g), maximum barrier height (W_m) and Crystallite size for S1, S2, S3 samples

Sample	Energy gap (E_g) (eV) [15]	W_m (eV)	Crystallite size (nm) [15]
S_1	2.75	2.317	8.64
S_2	2.63	1.697	11.60
S_3	2.43	1.073	12.05
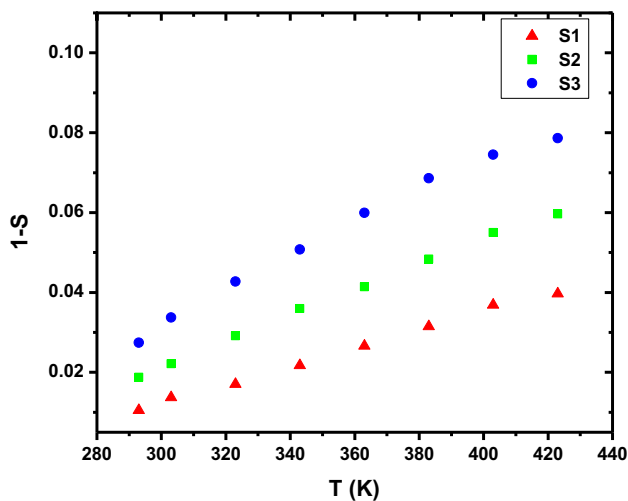
Figure 6 Temperature dependence of (1-S) for S1, S2 and S3 film samples.

For the determination of W_m, the parameter (1-s) is plotted as a function of temperature as seen in Fig. 6. The values of W_m, obtained from the straight lines seen in Fig. 6 are presented in Table 3. We can notice that W_m, decreases with the increase in the Cu
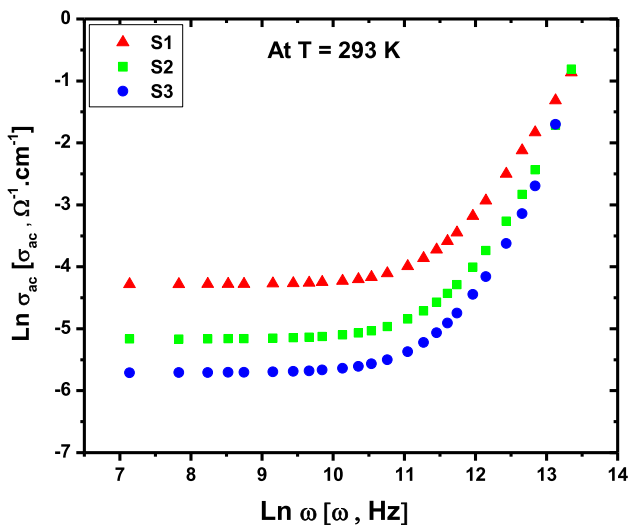
interlayer thickness, where similar behavior is observed for the optical energy gap of S1, S2 and S3 given in [15]. The observed values of ($W_m < Eg$), prove that the single polaron hopping mechanism becomes dominant [13].

The frequency dependence of the AC conductivity at room temperature for S1, S2 and S3 is given in Fig. 7 As seen, σ_{ac} increases with increasing frequency and decreases with the increase in the number of the Cu interlayer thickness. The observed change in σ_{ac} with Cu interlayer thickness is in a good agreement with the increase in crystallite size of the S1, S2 and S3 thin film samples, given previously in details in [15] and are summarized in Table 3. An increase in grain size decreases the density of contact area grain/grain, and hence the conductivity decreases due to growing hydrodynamic resistance.

The temperature dependence of AC conductivity for S1 as a function of versus 1000/T at different frequencies as a representative example is shown in Fig. 8.

The dependence of AC conductivity on temperature can be explained by the thermally activated process, in which the increase in temperature increasing the activation energy of the charge carriers and accordingly the AC conductivity increases. From Fig. 8, it is observed that ln σ_{ac} decreases with increasing the reciprocal temperature while increases by increasing frequency for S1, S2 and S3 samples. The values of the activation energies ΔE_{ac} of AC conductivity at different frequencies have been calculated from the slope of Ln σ_{ac} versus 1000/T curves
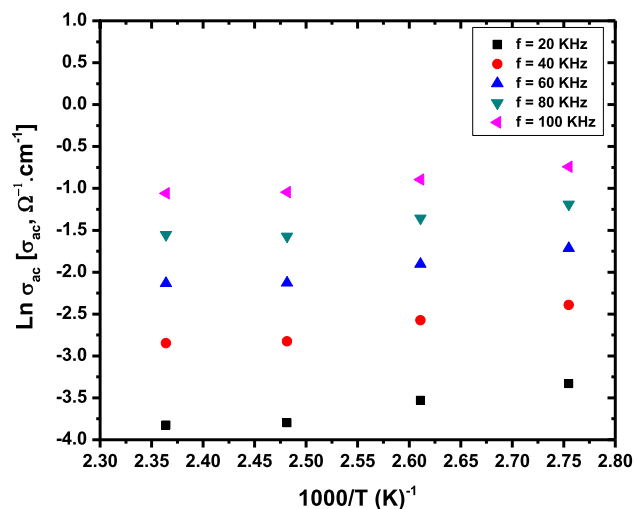

Figure 7 Ln σ_{ac} versus ln ω at room temperatures S1, S2 and S3.

Figure 8 Ln σ versus 1000/T at different frequencies for S1 as a representative example.
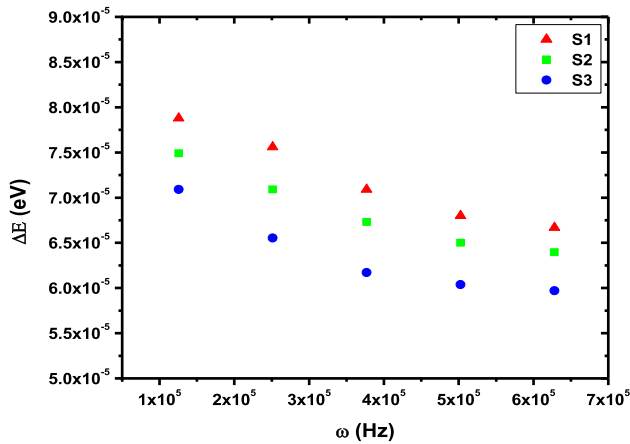
🍎 Springer

Figure 9 Frequency dependence of (ΔE) for S1, S2 and S3.

using Arrhenius equation. The variation of the activation energies ΔE_{ac} with different frequencies for S1, S2. S3 samples are represented in Fig. 9. The value of the activation energy is found to be dependent on the Cu interlayer thickness, were ΔE_{ac} exhibits a decrease with increasing both frequency and Cu thickness, that could be attributed to the applied field frequency that enhances the electronic jumps between localized states [29, 30].

Sheet resistance of ZnO/Cu/ZnO multilayer films

The sheet resistance (also known as surface resistance) is a critical property for any thin film of materials. The key advantage of sheet resistance over other resistance measurements is that it is independent of the size of the sample, thus enabling an easy way for comparison between different samples. The
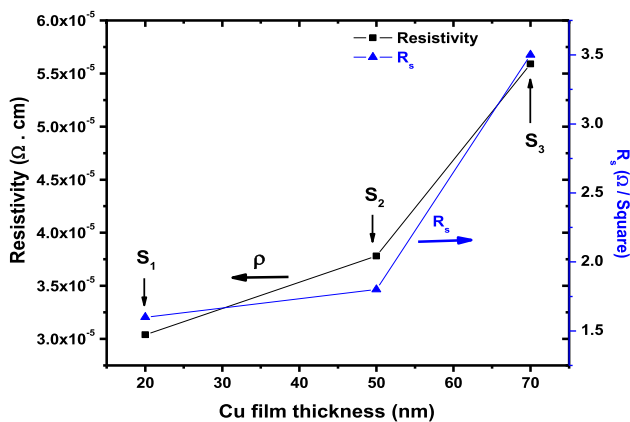

Figure 10 Resistivity and average sheet resistance versus Cu layer thickness at room temperature.

sheet resistance of ZnO/Cu/ZnO thin film system can be easily assessed using 4-point probe technique. Figure 10 illustrates the behavior of the sheet resistance and resistivity for S1, S2 and S3 thin film samples as a function of the Cu interlayer thickness at room temperature.

It is clearly observed that, the sheet resistance increases gradually according to an increase in the thickness of Cu interlayer. This is due to the grain growth of the crystallite size of our S1, S2 and S3 thin film samples given in [15] and in accordance with [31] as well. The variation of the resistivity parameters allows their potential utilization in these devices which are operated at high frequency. Upon Cu doping, a decrease in Eg occurs from 2.75 to 2.43 eV, and the nature of the optical transition were performed, also some physical quantities such as optical density, skin depth and refractive index were estimated, in order to determine the metallization criterion as given in details in [15]. These results confirm that the optical and electrical properties of ZnO/Cu/ZnO thin films depending on the thickness of the Cu interlayer and the crystalline improvement, i.e., by increasing the crystallite size from 8.64 to 12.05 nm with the increase of Cu%. The conductivity is the inverse or reciprocal of resistivity. The obtained results are in a good agreement with the reported results of the frequency dependence of σ_{ac} for S1, S2 and S3 film samples at room temperature given in Fig. 7 with that in Fig. 10. And also, in a good agreement with the data given in [15] for the crystallite size of our S1, S2 and S3 thin film samples.

Microhardness testing of ZnO/Cu/ZnO thin films

Hardness is the property of a material that allows it to resist permanent distortion penetration. Hardness testing is divided into two ranges: macrohardness and microhardness. Macrohardness testing with an applied load over 1 kg or about 10 Newton (N), while microhardness testing with applied loads under 10N, and is commonly used to measure hardness in very local area or small samples. The most common techniques used for microhardness are Vickers and Knoop hardness tests, and it is done on a microscopic scale with higher precision instruments. The Vickers microhardness were measured by using Japan's Shimadzu microhardness tester, with a force of 1.96 N over a period of 15 s. Normally, the entire load is

🖄 Springer

Table 4 Average hardness for S1, S2 and S3

Sample	Trail 1	Trail 2	Trial 3	Average hardness
S1	668	621	642	643.6
S2	564	574	530	556
S3	500	538	535	524.3

applied for 10 to 15 s for each sample. The Vickers hardness calculated by dividing the load by the indentation's square millimeter area. Three randomly indentation was tested on the same smooth surface for each sample [32, 33].

It is seen that; the microhardness decreases with increasing Cu thickness as shown in Table 4. This decrease in hardness may be due to the decrease in packing density. It means there was breaking of some bonds per volume in the material (ZnO) network during the application of load, which led to a decrease in the resistance of deformation. These results are in harmonic with the ZnO transition temperature [31]. The literature reports that the microhardness is inversely proportional to the grain size. Our results confirm the previous reports by comparing the increase in the grain size of the three samples of The ZnO/Cu/ZnO thin films with the decrease in the microhardness data of the same samples given in Table 4.

Conclusion

The proposed methodology of synthesis of the ZnO/Cu/ZnO thin films using the (ALD) technique and Dc magnetron sputtering methods proved to be very effective. By using suitable thickness of upper and lower ZnO layer with different Cu interlayer thickness we can achieve excellent electrical and mechanical properties. To determine the reason for the improvement of the AC conductivity and other related parameters the (GIXRD) was performed. The AC conductivity has been studied as a function of frequency and temperature. The results of the temperature dependence of AC conductivity were explained in terms of the correlated barrier hopping model (CBH). The 4-point Probes Resistivity Measurement System was used to investigate the electrical properties. The microhardness and the sheet resistance were also studied and showed a decrease with increasing Cu mid-layer thickness. By fitting the experimental data obtained from electrical and mechanical characteristic of ZnO/Cu/ZnO multilayer films, the results, are found to be highly composition dependent. These comprehensive results may be due to the crystalline improvement, i.e., increasing the Cu interlayer, reducing the defects such as dislocation interstitial, vacancy and interstitial.

Author contribution

S.S. Fouad:- The idea and the writing and the revision. Eszter Baradács and Bence Parditka:- Prepared samples and made the characterizations. N.F.Osman and M.E.Sayed:- Calculated the different parameters and prepared the results. L.I.Soliman:- Following up all the measurements and Revision. M.Nabil:- Prepared all the figures in the final form and responsible on the correspondence. Zoltán Erdélyi:- Prepared and supervising all the characteristics that had been made in Debrecen.

Data availability

All data generated or analyzed during this study are included in this published article.

Declarations

Conflict of interest The authors declare that they have no conflict of interest.

Ethical approval Not applicable.

References

[1] Li W-Y, Jiang L-X, Yin G-L, Wang Y-Y, Zhen Yu, He D-N (2013) Preparation and characterization of ZnO/Cu/ZnO transparent conductive films. Rare Met 32(3):273–277

[2] Lonescu ML, Bensebaa F, Luan BL (2012) ZnO/Cu/ZnO multilayers deposited on flexible substrate. Thin Solid Films 525:162–166

[3] Vidyasagar CC, Hosamani G, Kariyajjanavar P (2019) Optical and electrical properties of Cu-ZnO prism shape nanocrystals by microwave combustion method. Am J Energy Res 7(1):31–40

[4] Hanaa Z, Parditka B, Erdélyi Z, Atyia HE, Sharma P, Fouad SS (2020) Investigation of dispersion parameters, dielectric properties and opto–electrical parameters of ZnO thin film grown by ALD. Optik 203:163933

[5] Zayed H, Sayed ME, Elokr MM, Soliman LI (2018) Synthesis and characterization of Li_2O modified sodium phosphate glasses. J Sci Res Sci 35(1):417–438

[6] Licurgo JSC, de Almeida Neto GR, Paes Junior HR (2020) Structural, electrical and optical properties of copper-doped zinc oxide films deposited by spray pyrolysis. Ceramica 88:284–290

[7] Fouad SS, Baradács E, Nabil M, Parditka B, Negm S, Erdélyi Z (2022) Microstructural and optical duality of TiO_2/Cu/TiO_2 trilayer films grown by atomic layer deposition and DC magnetron sputtering. Inorg Chem Commun 145:110017

[8] Mehta N, Fouad SS, Baradacs E, Parditka B, Atyia HE, Pal SK, Erdelyi Z (2023) Multilayer stack structural designing of titania and Zinc white using atomic layer deposition (ALD) technique and study of thermally governed dielectric dispersion and conduction under alternating electric fields. J Mater Sci Mater Electron 34:708

[9] Hanaa Z, Fouad SS, Parditka B, Bekheet AE, Atyia HE, Medhat M, Erdélyi Z (2020) Enhancement of dispersion optical parameters of Al_2O_3/ZnO thin films fabricated by ALD. Sol Energy 205:79–87

[10] Fouad SS, Parditka B, Bekheet AE, Atyia HE, Erdélyi Z (2021) ALD of TiO_2/ZnO mutilayers towards the understanding of optical properties and polarizability.". Opt Laser Technol 140:107035

[11] Fouad SS, Bence Parditka HE, Atyia EB, Erdélyi Z (2022) The real role of Cu metallic interlayer on the dielectric dispersion and conduction mechanism of TiO_2/Cu/TiO_2 nanolaminates. Optik 260:169078

[12] Fouad SS, Parditka B, Nabil M, Baradács E, Negm S, Atyia HE, Erdélyi Z (2021) Bilayer number driven changes in polarizability and optical property in ZnO/TiO_2 nanocomposite films prepared by ALD. Optik 233:166617

[13] Fouad SS, Parditka B, Atyia HE, Baradács E, Bekheet AE, Erdélyi Z (2022) AC conductivity and dielectric parameters studies in multilayer TiO_2/ZnO thin films produced via ALD technique. Chin J Phys 77:73–80

[14] Modwi A, Taha KK, Khezami L, Boudina M, Khairy M, Al-Duaij OK, Talab S (2021) " Dependence of the electrical properties of Cu-doped ZnO nanoparticles decorated by Ag atoms. Z Phys Chem 235(6):745–767

[15] Fouad SS, Bence Parditka M, Nabil EB, Negm S, Erdélyi Z (2022) Effect of Cu interlayer on opto-electrical parameters of ZnO thin films. J Mater Sci Mater Electron 33:20594–20603

[16] Choudhary S, Sengwa RJ (2017) Morphological, structural, dielectric and electrical properties of PEO–ZnO nanodielectric films. J Polym Res 24(3):1–12

[17] Das HS, Gourisankar R, Kumar P, Das R (2021) Study the Effect of ZnO/Cu/ZnO multilayer structure by RF magnetron sputtering for flexible display applications.". ES Energy Environ 13:50–56

[18] Haga K, Kamidaira M, Kashiwaba Y, Sekiguchi T, Watanabe H (2000) ZnO thin films prepared by remote plasma-enhanced CVD method. J Cryst Growth 214:77–80

[19] Cruz-Gandarilla F, Morales-Acevedo A, Vigil O, Hesiquio-Garduno M, Vaillant L, Contreras-Puente G (2003) Microstructural characterization of annealed cadmium–zinc oxide thin films obtained by spray pyrolysis. Mater Chem Phys 78(3):840–846

[20] Jimenez-Gonzalez AE, Urueta JAS, Suarez-Parra R (1998) Optical and electrical characteristics of aluminum-doped ZnO thin films prepared by solgel technique. J Cryst Growth 192(3–4):430–438

[21] Zhu BL, Sun XH, Zhao XZ, Su FH, Li GH, Wu XG, Wu J, Wu R, Liu J (2008) The effects of substrate temperature on the structure and properties of ZnO films prepared by pulsed laser deposition. Vacuum 82(5):495–500

[22] Sahu DR, Huang J-L (2006) High quality transparent conductive ZnO/Ag/ZnO multilayer films deposited at room temperature. Thin Solid Films 515(3):876–879

[23] Bonse J, Wrobel JM, Kautek W (2000) Appl Phys A Mater Sci Process 72:89–94

[24] Graça MPF, Valente MA, da Ferreira-Silva MG (2003) Electrical properties of lithium niobium silicate glasses. J Noncryst Solids 325(1–3):267–274

Springer

[25] Ganaie M, Zulfequar M (2015) Study of density of localized states in $Cd_4Se_{96}-xSx$ (x= 0, 4, 8, 12) chalcogenide semiconductor. J Phys Chem Solids 85:51–55

[26] Wei J, Kobayashi A (2005) Research of TiN coatings by means of gas tunnel type plasma reactive spraying. Novel materials processing by advanced electromagnetic energy sources. Elsevier, New York, pp 427–432

[27] Mikla VI, Mikla VV (2011) Amorphous chalcogenides: the past present and future. Elsevier, New York

[28] Angell CA (1992) Mobile ions in amorphous solids. Ann Rev Phys Chem 43(1):693–717

[29] Sharma A, Mehta N, Kumar A (2011) Dependence of activation energy and pre-exponential factor on audio frequency in glassy $Se_{80}-xTe_{20}Sn_x$ alloys. J Alloys Compd 509(8):3468–3472

[30] Sanon G, Rup R, Mansingh A (1990) Growth and characterization of tin oxide films prepared by chemical vapour deposition. Thin Solid Films 190(2):287–301

[31] Sawamera S, Wondraczek L (2018) Phys Rev Mater 2:1–5

[32] Grabco DZ, Shikimaka OA, Elisa M, Sava BA, Bonroica L, Pyrtsak K, Prisacaru A, Danitsa Z, Feraru I, Ursu D (2012) Surf Eng Appl Eectrochem 48(4):365–374

[33] Miah MJ, Hossain AKM (2016) Magnetic, dielectric and complex impedance properties of $XBa_{0.95}.SR_{0.05}.TiO_3$—$(1-x)$ $BiFe_{0.9}Gd_{0.1}O_3$ multiferroic ceramics. Acta Metall Sin (English Letters) 29(6):505–517

Terms and Conditions

Springer Nature journal content, brought to you courtesy of Springer Nature Customer Service Center GmbH ("Springer Nature").

Springer Nature supports a reasonable amount of sharing of research papers by authors, subscribers and authorised users ("Users"), for small-scale personal, non-commercial use provided that all copyright, trade and service marks and other proprietary notices are maintained. By accessing, sharing, receiving or otherwise using the Springer Nature journal content you agree to these terms of use ("Terms"). For these purposes, Springer Nature considers academic use (by researchers and students) to be non-commercial.

These Terms are supplementary and will apply in addition to any applicable website terms and conditions, a relevant site licence or a personal subscription. These Terms will prevail over any conflict or ambiguity with regards to the relevant terms, a site licence or a personal subscription (to the extent of the conflict or ambiguity only). For Creative Commons-licensed articles, the terms of the Creative Commons license used will apply.

We collect and use personal data to provide access to the Springer Nature journal content. We may also use these personal data internally within ResearchGate and Springer Nature and as agreed share it, in an anonymised way, for purposes of tracking, analysis and reporting. We will not otherwise disclose your personal data outside the ResearchGate or the Springer Nature group of companies unless we have your permission as detailed in the Privacy Policy.

While Users may use the Springer Nature journal content for small scale, personal non-commercial use, it is important to note that Users may not:

1. use such content for the purpose of providing other users with access on a regular or large scale basis or as a means to circumvent access control;

2. use such content where to do so would be considered a criminal or statutory offence in any jurisdiction, or gives rise to civil liability, or is otherwise unlawful;

3. falsely or misleadingly imply or suggest endorsement, approval , sponsorship, or association unless explicitly agreed to by Springer Nature in writing;

4. use bots or other automated methods to access the content or redirect messages

5. override any security feature or exclusionary protocol; or

6. share the content in order to create substitute for Springer Nature products or services or a systematic database of Springer Nature journal content.

In line with the restriction against commercial use, Springer Nature does not permit the creation of a product or service that creates revenue, royalties, rent or income from our content or its inclusion as part of a paid for service or for other commercial gain. Springer Nature journal content cannot be used for inter-library loans and librarians may not upload Springer Nature journal content on a large scale into their, or any other, institutional repository.

These terms of use are reviewed regularly and may be amended at any time. Springer Nature is not obligated to publish any information or content on this website and may remove it or features or functionality at our sole discretion, at any time with or without notice. Springer Nature may revoke this licence to you at any time and remove access to any copies of the Springer Nature journal content which have been saved.

To the fullest extent permitted by law, Springer Nature makes no warranties, representations or guarantees to Users, either express or implied with respect to the Springer nature journal content and all parties disclaim and waive any implied warranties or warranties imposed by law, including merchantability or fitness for any particular purpose.

Please note that these rights do not automatically extend to content, data or other material published by Springer Nature that may be licensed from third parties.

If you would like to use or distribute our Springer Nature journal content to a wider audience or on a regular basis or in any other manner not expressly permitted by these Terms, please contact Springer Nature at

onlineservice@springernature.com